PHYSICAL REVIEW B **80**, 174424 (2009)

Magnetic structure of $EuFe_2As_2$ determined by single-crystal neutron diffraction

Y. Xiao,[1,*] Y. Su,[2] M. Meven,[3] R. Mittal,[2,4] C. M. N. Kumar,[1] T. Chatterji,[5] S. Price,[2] J. Persson,[1] N. Kumar,[6] S. K. Dhar,[6] A. Thamizhavel,[6] and Th. Brueckel[1,2,5]

[1]*Institut fuer Festkoerperforschung, Forschungszentrum Juelich, D-52425 Juelich, Germany*

[2]*Juelich Centre for Neutron Science, IFF, Forschungszentrum Juelich, Outstation at FRM II, Lichtenbergstrasse 1, D-85747 Garching, Germany*

[3]*FRM II, Technische Universitaet Muenchen, Lichtenbergstrasse 1, D-85747 Garching, Germany*

[4]*Solid State Physics Division, Bhabha Atomic Research Centre, Trombay, Mumbai 400 085, India*

[5]*Juelich Centre for Neutron Science, Forschungszentrum Juelich, Outstation at Institut Laue-Langevin, BP 156, 38042 Grenoble Cedex 9, France*

[6]*Department of Condensed Matter Physics and Material Sciences, Tata Institute of Fundamental Research, Homi Bhabha Road, Colaba, Mumbai 400 005, India*

(Received 28 August 2009; revised manuscript received 30 October 2009; published 25 November 2009)

Among various parent compounds of iron pnictide superconductors, $EuFe_2As_2$ stands out due to the presence of both spin density wave of Fe and antiferromagnetic (AFM) ordering of the localized Eu^{2+} moment. Single-crystal neutron-diffraction studies have been carried out to determine the magnetic structure of this compound and to investigate the coupling of two magnetic sublattices. Long-range AFM ordering of Fe and Eu spins was observed below 190 and 19 K, respectively. The ordering of Fe^{2+} moments is associated with the wave vector $\mathbf{k}=(1,0,1)$ and it takes place at the same temperature as the tetragonal to orthorhombic structural phase transition, which indicates the strong coupling between structural and magnetic components. The ordering of the Eu moments is associated with the wave vector $\mathbf{k}=(0,0,1)$. While both Fe and Eu spins are aligned along the long *a* axis as experimentally determined, our studies suggest a weak coupling between the Fe and Eu magnetism.

DOI: 10.1103/PhysRevB.80.174424 PACS number(s): 75.25.+z, 75.50.Ee, 74.70.−b

I. INTRODUCTION

The recent discovery of pnictide superconductors has drawn extensive attention because it provides an opportunity to investigate the mechanism of superconductivity.[1–4] Most of the research on pnictide superconductors has focused on RFeAs($O_{1-x}F_x$) (with R=La, Nd, Sm, or Pr, etc.) and AFe$_2$As$_2$ (with A=Ba, Ca, or Sr, etc.), the so called "1111" and "122" families. These two families are closely related since both of them adopt a layered structure with a single FeAs layer in the unit cell of 1111 and two such layers in the unit cell of "122." The superconducting state can be achieved either by electron or hole doping of the parent compounds.[5–7] Apart from carrier doping, the application of hydrostatic pressure or chemical pressure can also induce superconductivity.[8,9] Considering that the electronic states near the Fermi surface are dominated by contributions from Fe and As, it is believed that the FeAs layers are responsible for superconductivity in these compounds.

Recent neutron diffraction experiments reveal that the formation of the spin density wave (SDW), originating from the long-range antiferromagnetic (AFM) order of the Fe moments at low temperature, seems to be a common feature for all the iron pnictide parent compounds.[10–13] The onset of the AFM order is also accompanied by the tetragonal-orthorhombic (T-O) structural phase transition in the 122 family and preceded by the T-O phase transition for the 1111 family. Phase diagrams of some iron pnictides clearly show that the magnetic order is suppressed with appropriate charge carrier doping of parent compound. Concomitantly, superconductivity emerges and reaches a high T_c at optimal doping,[14] thus exhibiting features similar to high T_c cuprates.[15]

$EuFe_2As_2$ is a peculiar member of iron arsenide AFe$_2$As$_2$ family since the A site is occupied by Eu^{2+}, which is an S-state rare-earth ion possessing a $4f^7$ structure with the electron spin $S=7/2$.[16] As revealed by Mössbauer and magnetic susceptibility measurement on single crystals, the Eu^{2+} moments order antiferromagnetically below $T_N\sim 20$ K and A-type AFM ordering of Eu^{2+} spins is proposed.[17,18] It is reported that the superconductivity can be achieved by replacing Eu by alkali metals or replacing As by P, e.g., the T_c is observed to be 31 and 26 K for $Eu_{0.5}K_{0.5}Fe_2As_2$ (Ref. 19) and $EuFe_2(As_{0.7}P_{0.3})_2$,[9] respectively. In $EuFe_2(As_{0.7}P_{0.3})_2$, the superconducting transition is found to be followed by ferromagnetic order of Eu^{2+} moment, which indicates the coexistence of superconductivity and magnetism.[9]

Since magnetism and superconductivity appears to be intimately related in iron pnictides, it is therefore equally important to understand the magnetic properties especially for the compounds that contain the magnetic lanthanide ions. The investigation of the interplay between the lanthanide and iron magnetism may also be crucial for a deeper understanding of the magnetic and electronic properties of iron pnictides. For $EuFe_2As_2$, the magnetic ordering and the details of magnetic structure have not been clarified so far via single-crystal neutron diffraction due to the extremely large neutron absorption cross-section of Eu. Here we report neutron-diffraction studies on a high-quality $EuFe_2As_2$ single-crystal using the hot-neutron source. It has been observed that both the Fe^{2+} and Eu^{2+} moments are ordered antiferromagnetically below 190 and 19 K, respectively. A unique propagation vector $\mathbf{k}=(1,0,1)$ is determined for the Fe magnetic

sublattice with the moment aligned along the *a* axis. Furthermore, the magnetic propagation vector is determined to be $\mathbf{k}=(0,0,1)$ for the Eu^{2+} moment, which is also aligned along the *a* axis. The coupling between the Fe and Eu magnetic sublattices has been found to be rather weak. The determination of the magnetic structure of $EuFe_2As_2$ would pave the way for further investigations of $EuFe_2As_2$ under high pressure and strong magnetic fields.

II. EXPERIMENT

The single crystals of $EuFe_2As_2$ were grown by the high temperature solution growth method using a fourth element, Sn as the solvent. Sn has been found to be a good solvent for the AFe_2As_2 (with A=Ba, Ca, Sr, and Eu) compounds which can dissolve the constituent metals and create a supersaturated solution at about 1050 °C. Here we have started with the charge of high purity individual metals Eu, Fe and As in the ratio 1:2:2 together with the solvent Sn with the flux to charge ratio 19:1. All the metals were placed in a recrystallized alumina crucible and sealed in a quartz ampoule with a partial pressure of argon gas. The sealed crucible was then slowly heated to 1050 °C and kept at this temperature for one day to achieve proper homogenization. Then the temperature of the furnace was cooled down to 500 °C over a period of three weeks. The grown crystals were extracted from the solvent Sn by means of centrifuging at 500 °C. Several platelet like single crystals with typical dimension $5\times5\times1$ mm^3, which were sticking to the walls of the crucible, were extracted by gently tapping the alumina crucible after centrifuging the flux. A small amount of powdered single-crystal was examined by means of x-ray powder diffraction (XRD) analysis. The XRD pattern reveals a single phase of $EuFe_2As_2$ in the tetragonal $ThCr_2Si_2$ structure with space group $I4/mmm$ at room temperature. The samples have also been characterized via the measurements of heat capacity, resistivity and magnetic susceptibility. Two prominent phase transitions can be identified respectively at 190 and 19 K, consistent to those previously reported.[17,18]

A 50 mg single-crystal with dimension about $5\times5\times1$ mm^3 was selected for neutron diffraction experiment, which was performed on hot-neutron four-circle diffractometer HEIDI at FRM II, Garching (Germany).[20] A Cu (220) monochromator was selected to produce a monochromatic neutron beam with the wavelength at 0.868 Å. An Er filter was used to minimize the $\lambda/2$ contamination. The single-crystal sample was mounted on a thin aluminum holder inside a standard closed-cycle cryostat. The diffraction data were collected using a ^{3}He single detector at different temperatures from 300 K down to 2.5 K. A fine collimation ($\sim15'$) in front of the sample and a narrow opening of the detector slits were adopted to achieve a sufficient resolution, in order to determine precisely the structural splitting due to orthorhombic twinning and magnetic modulation wave vectors. To ensure the inclusion of the contributions from all possible twinned domains, the integrated intensities were collected with the setup adopting a 60′ collimation and an angular opening of both horizontal and vertical detector slits set at 4.5°. Furthermore, the integrated intensities for the reflections with $2\theta>60°$ and $2\theta<60°$ were obtained, respectively, via the θ-2θ and the rocking-curve scans. The obtained data used for the structural refinements were normalized by monitor counts and corrected for the Lorentz factor. DATAP program is used to carry out absorption correction by considering the size and shape of crystal.[21] The absorption coefficient μ is calculated to be 2.61 mm^{-1} and the transmission factors are deduced to be only in the range from 2.1% up to 14.2% due to the extremely strong absorption. Refinement of both the nuclear and magnetic structures was performed by using the FULLPROF program suit.[22] The scale factor derived from the crystal structure refinement was used to determine the magnitude of magnetic moment from the magnetic reflections.

III. RESULTS AND DISCUSSION

First of all, the crystal structure of $EuFe_2As_2$ is described within the framework of tetragonal symmetry at 300 K. The ω scans of selected nuclear $(220)_T$ and $(200)_T$ reflections with mosaic width of $\sim0.22°$ are shown in Figs. 1(a) and 1(b), which indicate the good quality and homogeneity of the single-crystal. Upon cooling down, a splitting is observed for orthorhombic $(400)_O$ and $(040)_O$ reflections [Fig. 1(c)]. Note that those two reflections are corresponding to the $(220)_T$ in tetragonal setting according to the tetragonal-orthorhombic symmetry relation. The observed splitting of $(400)_O$ is the indication of T-O structural transition and accompanied twinning configuration due to the interchange of the orthorhombic *a* and *b* axes. It is known that twinning in orthorhombic structure will result in four different domain patterns,[23,24] as illustrated in Fig. 1(e). Two of domains shared the same (110) plane and formed the domain pairs (D1 and D2), while another two shared the $(\bar{1}10)$ plane (D3 and D4). In principle, it is possible to observe single peak, two or three or four peaks depending on the selected reflections and the resolution of the instrument. In Fig. 1(c), the left and right peaks can be assigned to the contributions from the domains (D1+D3) and (D2+D4), respectively. Note that the ω scan is performed with open detector slits. Two Gaussian peaks were used to fit the $(400)_O$ and $(040)_O$ reflections and the domain population ratio is estimated to be around 1:1 for the $(h00)$ and $(0k0)$ twins, i.e., D1+D3≈D2+D4. The ω scan of $(\bar{2}20)$ is examined afterward with the $(hk0)$ aligned in the horizontal scattering plane to obtain more detailed information about domain population [Fig. 1(d)]. The occurrence of twinning and T-O structural phase transition can be confirmed from the clear presence of triple splitting of $(\bar{2}20)$ nuclear reflection. Usually, the reflections with $h=k\neq0$ are triply split in twinned orthorhombic lattice and the peak in the center is attributed to pairs that share the same $(\bar{1}10)$ or (110) plane, while the peak at left and right sides corresponds to the rest two domains. In Fig. 1(d), it can be seen that all three peaks showed almost equal intensity. This strongly indicates that the domain population exists the following relationship: D1≈D3+D4≈D2. Hence the domain population for all those four different domain patterns can be determined roughly as 2:2:1:1. In order to investigate the distri-

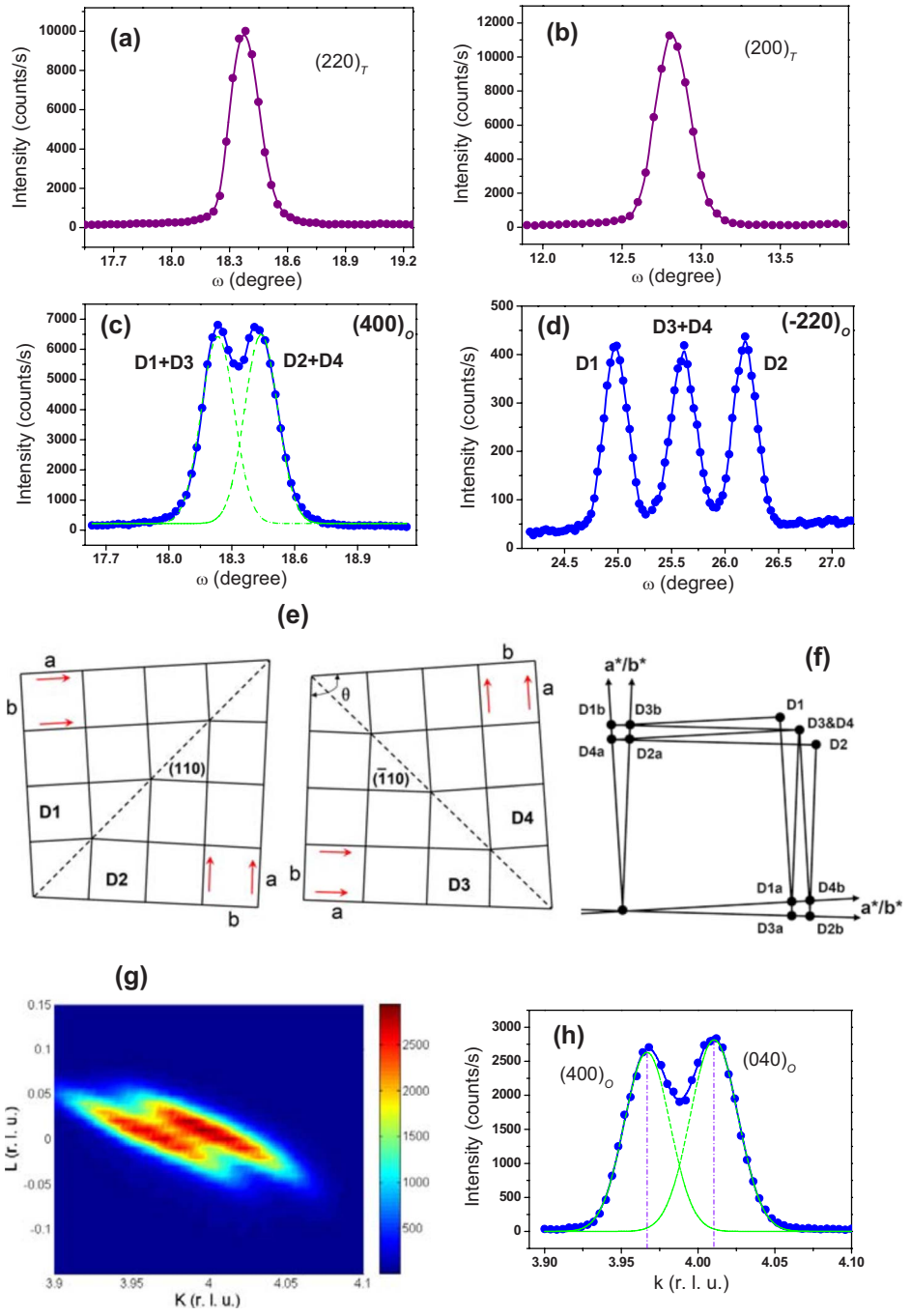

FIG. 1. (Color online) (a) and (b) Omega scans of tetragonal $(220)_T$ and $(400)_T$ nuclear reflection at 300 K, respectively. (c) Omega scan of orthorhombic $(400)_O$ nuclear reflection at 2.5 K. The splitting of the reflection indicates the existence of twinned domains. (d) Triple splitting of the rocking curve of orthorhombic $(\bar{2}20)_O$ reflection at 2.5 K, as measured with the $(hk0)$ aligned nearly in the horizontal scattering plane. (e) Schematic presentation of the twinned orthorhombic lattice in real space. Four domain patterns are marked as D1–D4. a and b denote long and short axis of orthorhombic lattice. Arrows indicate the direction of the Fe magnetic moment. (f) Schematic presentation of the reciprocal space corresponding to the twinned orthorhombic domains. (g) The contour map of orthorhombic $(400)_O$ reflection at 2.5 K. (h) Q scan of $(400)_O$ reflection.

bution of nuclear reflection in reciprocal space and determine the lattice parameter accurately, two-dimensional plot of $(400)_O$ reflection is shown in Fig. 1(g). The splitting of $(400)_O$ can also be clearly seen. Totally 280 nuclear reflections were collected for nuclear structure refinement within the *Fmmm* space group. A single extinction parameter was applied in FULLPROF code for correction of the extinction and several strong reflections were excluded from the refinement because of the significant extinction. All atoms were refined with the isotropic temperature factor. The refinement results of the crystal structure are listed in Table I. The lattice parameters are deduced to be $a=5.537(2)$ Å, $b=5.505(2)$ Å, and $c=12.057(2)$ Å at 2.5 K, which are in good agreement with a previous report.[25]

TABLE I. Refined results of the crystal and magnetic structures for $EuFe_2As_2$ at 2.5 K (space group: *Fmmm*, $Z=4$).

Atom/site	x	y	z	B (Å^2)
Eu (4*a*)	0	0	0	0.81(3)
k, $M_a(\mu_B)$	(0,0,1), 6.8(3)			
Fe (8*f*)	0.25	0.25	0.25	0.26(3)
k, $M_a(\mu_B)$	(1,0,1), 0.98(8)			
As (8*i*)	0	0	0.363(5)	0.25(3)
a, *b*, *c* (Å): 5.537(2), 5.505(2), 12.057(2)				
Number of reflections (Nuclear): 280				
RF^2, RF^{2W}, $RF(\%)$, χ^2 Nuclear: 9.34, 9.67, 6.22, 7.1				
Number of reflections (Magnetic): 228				
RF^2, RF^{2W}, $RF(\%)$, χ^2 Magnetic: 9.42, 7.68, 6.53, 5.7				

To clarify the magnetic structure of $EuFe_2As_2$ at low temperature, the sample was cooled to 2.5 K, which is well below the reported Fe^{2+} and Eu^{2+} magnetic ordering temperatures. Considering the existence of the twinned (*h*00) and (0*k*0) domains, extensive search of magnetic reflections was performed in the a^*-c^* reciprocal space as schematically illustrated in Fig. 2(a). Additional search was also performed in the (*hhl*) reciprocal plane. Figure 2(b) shows three typical long *l* scans in the reciprocal space where in addition to the expected nuclear reflections, two sets of magnetic superstructure reflections can be clearly identified with two magnetic propagation wave vectors (1,0,1) and (0,0,1), respectively. As an example, *Q* scan of $(101)_M$ magnetic reflection is plotted in Fig. 3(a) and the same scan at 200 K is also plotted together for comparison. In Fig. 3(b), the θ-2θ scan of nuclear $(002)_N$ and magnetic $(003)_M$ reflections show the same peak center, which indicates that the magnetic structure is commensurate in nature. The contour map of $(103)_M$ and $(401)_M$ reflections fully illustrated the intensity distribution as shown in Figs. 3(c) and 3(e). As already discussed, the contour map of $(400)_O$ nuclear reflection [Fig. 1(g)] clearly shows two reflections attributed to the (*h*00) and (0*k*0) twins. Two peak centers with $k=3.967$ and 4.01 can be obtained by fitting the *Q* scan of $(400)_O$ reflection [Fig. 1(h)]. In Fig. 3(d), the *Q* scan of $(103)_M$ reflection can be fitted by a single Gaussian function with $k=0.991$. This strongly indicates that the (*h*0*l*) type reflections (with *h* and *l* equal to odd number) are associated with the (*h*00) domain and they can thus be described with the propagation wave vector $\mathbf{k}=(1,0,1)$. This wave vector is exactly the same as observed in other 122 pnictides, such as $BaFe_2As_2$ (Ref. 12) and $CaFe_2As_2$,[13] which is related to the AFM order of Fe^{2+} moments. The magnetic structure refinement was then carried out to determine the magnitude and direction of Fe^{2+} moment. The magnetic structure with Fe saturation moment of 0.98(8) μ_B aligned along the long *a* axis is deduced.

Consequently, the magnetic reflections with a propagation wave vector $\mathbf{k}=(0,0,1)$ (with *h* even and *l* odd) are due to the long-range order of the localized Eu^{2+} moments. However, the moment direction of Eu^{2+} moments is still indeterminate. Symmetry analysis based on the representation

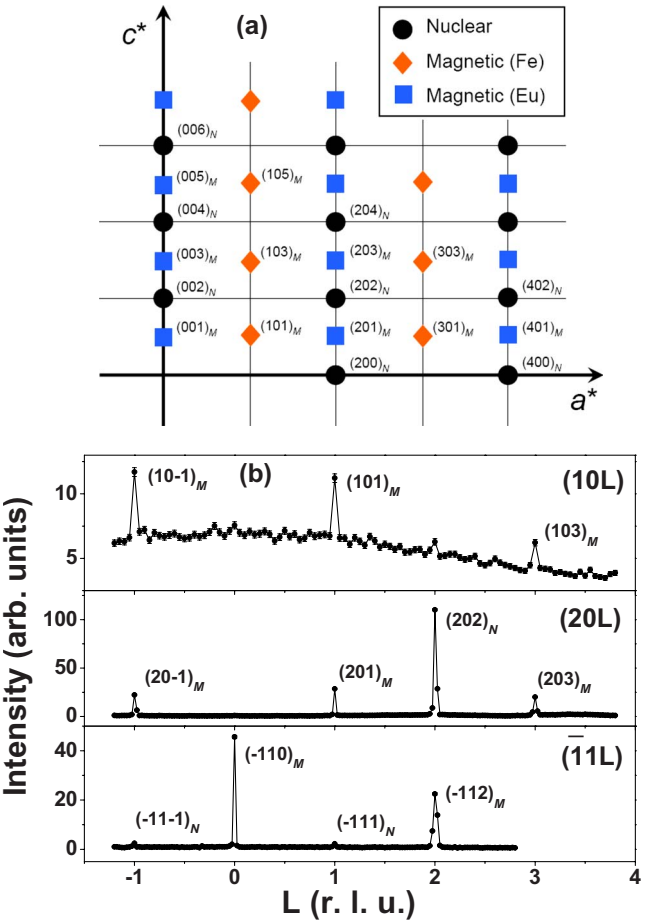

FIG. 2. (Color online) (a) The schematic diagram of (*h*0*l*) plane in the first quadrant of reciprocal space. The circular, rhombic, and square symbols represent the nuclear reflection as well as the magnetic reflection attributed to Fe and Eu magnetic sublattices. (b) Long *l* scan on (01*l*), (02*l*), and ($\bar{1}$1*l*) reflections.

theory indicates that the magnetic representation Γ for magnetic Eu^{2+} on 4*a* site is decomposed into three one dimensional irreducible representations: Γ_1, Γ_2, and Γ_3. The Eu^{2+} moments are aligned in the *c*, *a*, or *b* direction according to those three representations. The observation of nonzero intensity of (00*l*) (with *l*=odd) reflections clearly exclude the representation Γ_1. The ω scans on several $(hk0)_M$ (with both *h* and *k*=odd) reflections also exhibit considerable intensity. Thus, the moment of Eu^{2+} is expected to be aligned either along the *a* or *b* direction in the *ab* plane. The *Q* scan on $(041)_M$ reflection [Fig. 3(f)] giving a peak position of $k=4.01$, which is exactly equal to the larger *k* value of $(400)_O$ nuclear reflection. Therefore, the moment direction of Eu^{2+} can be determined as along the *a* direction since the intensity ratio between $(041)_M$ and $(401)_M$ magnetic reflections approximate equals to 73:1 for this arrangement. The structure mode is confirmed further by ω scan of series of (02*l*) (with *l*=odd) reflections as shown in Fig. 4. Similar to some nuclear reflections, both (20*l*) and (02*l*) magnetic reflections was detected due to the twinning configuration. However, the intensity ratio between (20*l*) and (02*l*) changes gradually with the change of the angle between the scattering plane and the *c* axis. The calculated intensity ratio of (20*l*)/(02*l*)

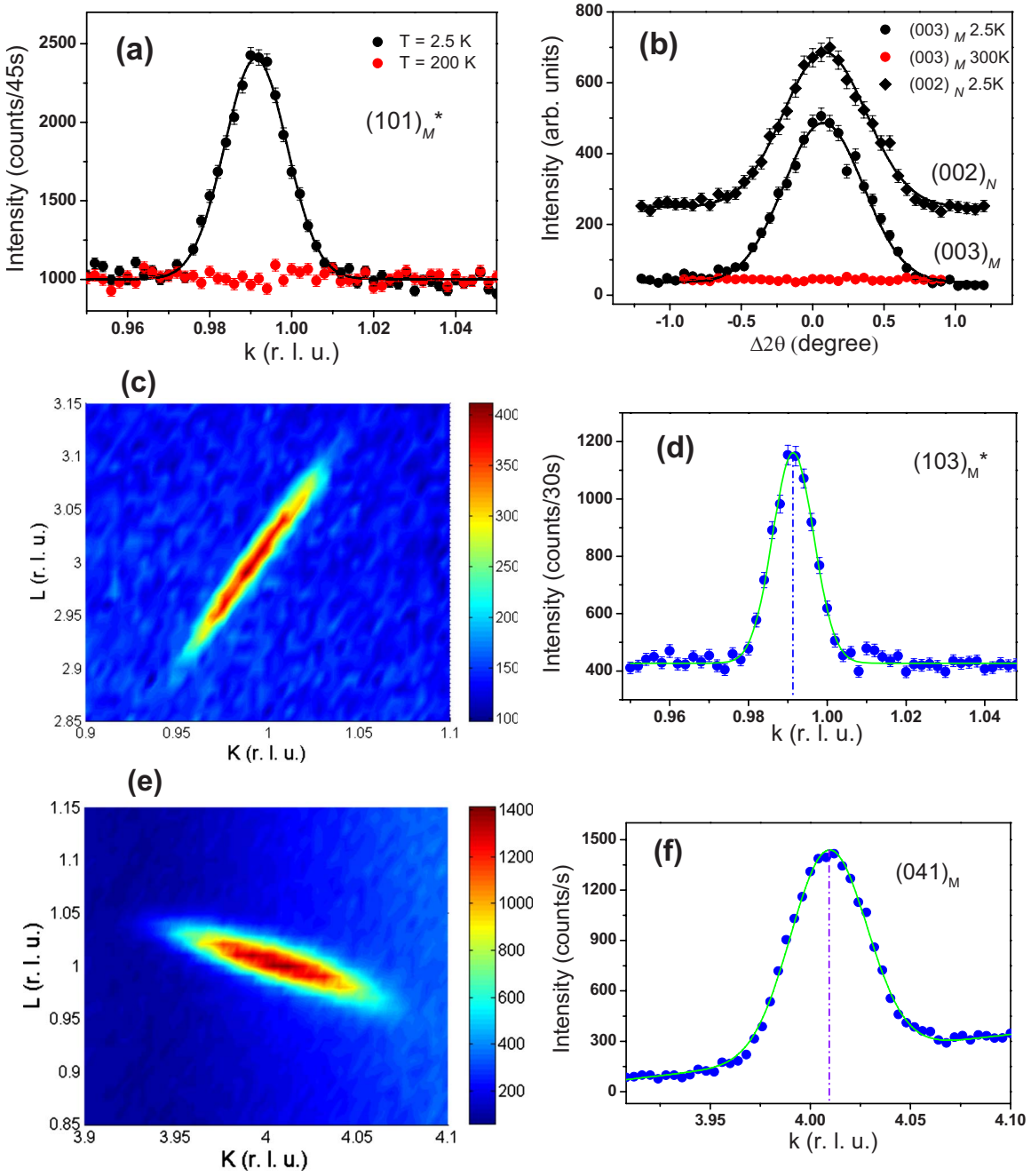

FIG. 3. (Color online) (a) The comparison of the Q scan of $(101)_M$ magnetic reflection at 2.5 and 200 K. The $(101)_M$ reflection is observed in k scan because of the existence of twinned domains. (b) The θ-2θ scan of $(003)_N$ nuclear and $(003)_M$ magnetic reflections at 2.5 K, the same scan of $(003)_M$ magnetic reflection at 300 K is also plotted for comparison. (c) The contour map shows the Q dependence of the $(103)_M$ magnetic reflection. (d) Q scan of $(103)_M$ magnetic reflection. The $(103)_M$ reflection is observed in k scan because of the existence of twinned domains. (e) The contour map of $(041)_M$ magnetic reflection indicates the contribution of the magnetic reflection of Eu magnetic sublattice. (f) Q scan of $(041)_M$ magnetic reflection.

for different l are plotted in Fig. 4(f) and it agrees well with the observed values which derived from the ω scans directly. By taking into account of twinned components properly, the refinement on Eu^{2+} magnetic sublattice was carried out with the aforementioned magnetic structure model. The calculated structure factors are plotted against those observed and shown in Fig. 5. The reliable agreement factors confirms the proposed magnetic structural model eventually, i.e., the Eu^{2+} moment aligns along a direction with the wave vector $\mathbf{k}=(0,0,1)$ and magnitude of 6.8(3) μ_B. Thus the magnetic structure of $EuFe_2As_2$ is unambiguously determined as illustrated in Fig. 6. The moment direction of Eu^{2+} is also consistent with our resonant x-ray scattering (RXS) measurement.[26] Parallel alignment of the Fe^{2+} and Eu^{2+} moments might be resulted from thermal or ground state fluctuations.

Figure 7(a) shows the temperature dependence of the $(112)_M$ and $(003)_M$ magnetic reflections attributed to the or-

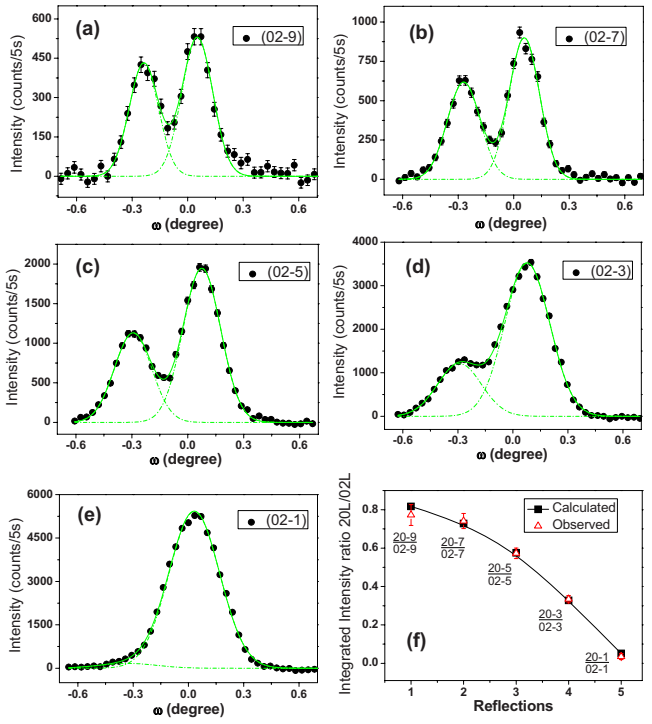

FIG. 4. (Color online) (a)–(e) Omega scans of series of (02l) (with l=odd) reflections at 2.5 K. The integrated intensities of (20l) and (02l) can be obtained by fitting the curves with two Gaussian functions. (f) The ratio between (20l) and (02l) reflections shows good agreement with the calculated value.

dering of Eu^{2+} moments. The onset temperature of Eu^{2+} magnetic order is deduced to be 19 K, which is in good agreement with previous report on electronic and magnetic measurements.[17,18] The magnetic ordering temperature of Fe^{2+} moment is estimated to be 190 K based on the temperature dependence of the $(101)_M$ and $(103)_M$ magnetic reflections [see Fig. 7(b)]. The T-O structural phase transition also takes place at 190 K as revealed by the sharp change of full width at half maximum (FWHM) in $(040)_O$ nuclear reflection. First-principle calculations suggest that the nearest- and next-nearest-neighbor superexchange interactions between

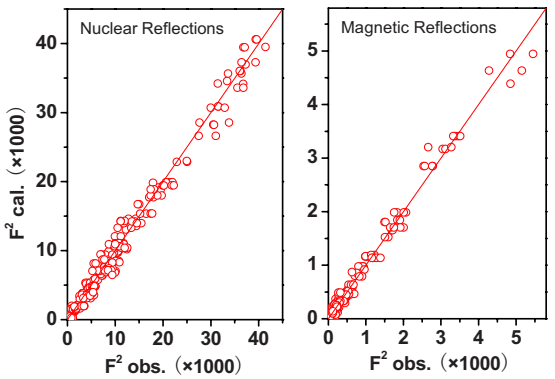

FIG. 5. (Color online) Integrated intensities of the nuclear and magnetic Bragg reflections collected at 2.5 K are plotted against the calculated values. See text for details of the crystal and magnetic structure models.

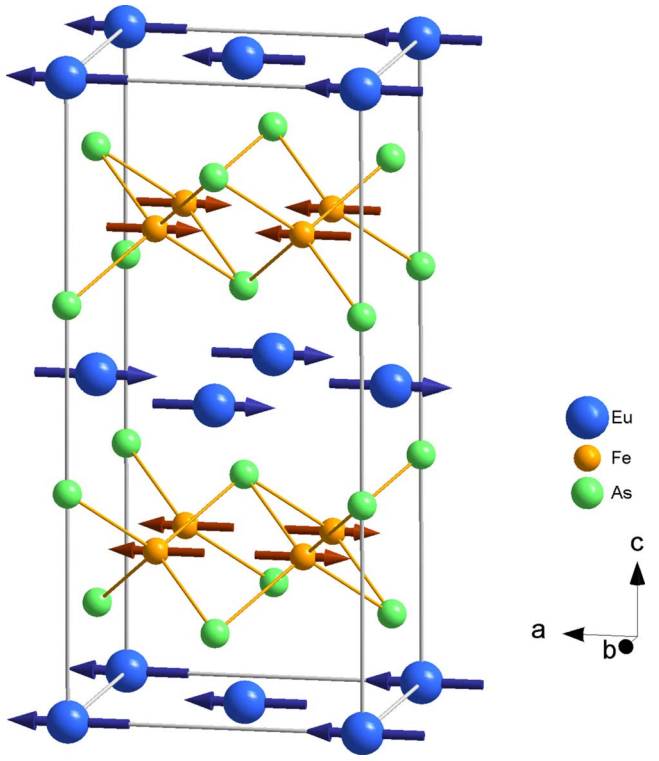

FIG. 6. (Color online) Illustration of the magnetic structures of $EuFe_2As_2$ at 2.5 K. The Fe moments align along a direction and order antiferromagnetically in both a and c directions. The Eu moments align along a direction and order antiferromagnetically in c direction only. The gray line outlines the orthorhombic unit cell.

Fe ions lead to a frustrated magnetic ground state in pnictides with parallel and antiparallel arrangement of Fe spins in FeAs layer.[27] Usually, the magnetic frustration can be lifted by a structural distortion from high-symmetry to low-symmetry phase. This may be the origin of the strong coupling between the structural and magnetic phase transitions observed in $EuFe_2As_2$ and other iron pnictides.[11–13]

Due to the localized nature of Eu 4f state, the AFM coupling of Eu^{2+} moments would be described by the indirect exchange, e.g., the Ruderman-Kittel-Kasuya-Yosida (RKKY) interaction as suggested for other $ThCr_2Si_2$-type

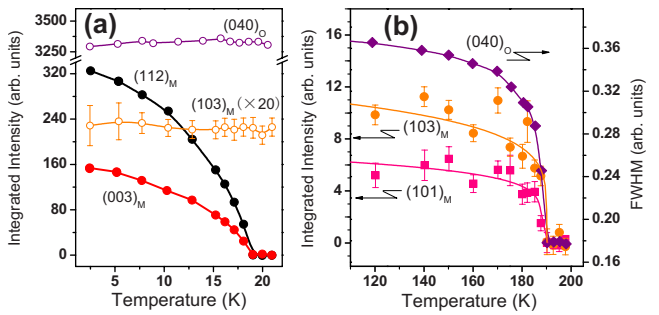

FIG. 7. (Color online) (a) Temperature dependence of integrated intensity of $(040)_O$ nuclear reflection as well as the $(103)_M$, $(112)_M$, and (003) magnetic reflections below 22 K. (b) Temperature dependence of integrated intensity of $(103)_M$ and $(101)_M$ reflections; temperature dependence of FWHM of $(040)_O$ reflection.

compounds.[28,29,32] However, the commensurate AFM structure of $EuFe_2As_2$ is different from that of some other isostructural Eu-based compounds, such as $EuCo_2P_2$ (Ref. 28) and $EuRh_2As_2$.[29] In $EuCo_2P_2$, the incommensurate AFM spiral structure with the wave vector $\mathbf{k}=(0,0,0.85)$ is determined, while the coexistence of commensurate [with $\mathbf{k}=(0,0,1)$] and incommensurate [with $\mathbf{k}=(0,0,0.9)$] AFM structure is observed in $EuRh_2As_2$ compound. The common feature for both commensurate and incommensurate phases is that the Eu moment ordered ferromagnetically in *ab* plane of unit cell. The band-structure calculation suggested that the propagation wave vector is associated with the valence of Eu ions:[29] the commensurate structure formed in the phase composed of the divalent Eu ions and incommensurate structure is originated from the phase with the anomalous valence state of Eu. Therefore, the Eu^{2+} in $EuFe_2As_2$ is fully localized and results in the commensurate AFM structure. It is also noticed that the valence of Eu ions is somehow related with the Eu-(As/P) bond length if we compare the c/a ratio and the Eu valence of $EuRh_2P_2(c/a=2.47, \nu=2.2)$, $EuRh_2As_2(c/a=2.77, \nu=2.13)$, and $EuFe_2As_2(c/a=3.09, \nu=2)$.[16,29–31] The variation in Eu valence with the change in bond length indicated that the Eu 4*f* electrons might participate in the Eu-(As/P) bonding and the electronic state between Eu ions and Fe(As/P) layers is strongly correlated. Thereby the RKKY exchange interaction might be modified by the change of electronic state of Fe(As/P) layers and thus leads to different magnetic structures. Indeed, the evidence on possible coupling between localized Eu^{2+} moments and itinerant electrons from two-dimensional FeAs layers is observed in $EuFe_{2-x}Ni_xAs_2$ system[32] and in $EuFe_2As_2$ by electron spin resonance.[33] However, in present neutron work, we did not observe any detectable change in Fe^{2+} magnetic moment when temperature is passing through the Eu^{2+} magnetic ordering temperature [Fig. 7(a)]. This may suggest the weak interaction between the Eu and Fe magnetic sublattices, which is supported by the full potential electronic structure calculation.[34] Further experimental work via complementary techniques and comprehensive band-structure calculations are necessary in order to clarify the exact nature of the interplay between the electronic state, Eu valence and itinerant and localized magnetism in Eu-based 122 compounds.

IV. CONCLUSION

Single-crystal neutron-diffraction experiment using a hot-neutron source was performed to investigate the crystal and magnetic structure of $EuFe_2As_2$. With decreasing temperature, the antiferromagnetic order of Fe^{2+} moments set in at 190 K with the propagation vector $\mathbf{k}=(1,0,1)$. Similar to $BaFe_2As_2$ and $CaFe_2As_2$, the tetragonal to orthorhombic structural transition occurs simultaneously with the AFM order, which indicates the strong coupling between the lattice and Fe magnetic degree of freedom. Below 19 K, the Eu^{2+} moments order antiferromagnetically with the propagation vector $\mathbf{k}=(1,0,1)$ and are aligned along the *a* axis. our studies also suggest a weak coupling between the Fe^{2+} and Eu^{2+} magnetic sublattice.

ACKNOWLEDGMENT

We would like to thank G. McIntyre from the Institut Laue-Langevin (France) for his kind help in the data analysis.

*y.xiao@fz-juelich.de

[1] Y. Kamihara, T. Watanabe, M. Hirano, and H. Hosono, J. Am. Chem. Soc. **130**, 3296 (2008).
[2] H. Takahashi, K. Igawa, K. Arii, Y. Kamihara, M. Hirano, and H. Hosono, Nature (London) **453**, 376 (2008).
[3] S. Matsuishi, Y. Inoue, T. Nomura, H. Yanagi, M. Hirano, and H. Hosono, J. Am. Chem. Soc. **130**, 14428 (2008).
[4] M. Rotter, M. Tegel, and D. Johrendt, Phys. Rev. Lett. **101**, 107006 (2008).
[5] H. H. Wen, G. Mu, L. Fang, H. Yang, and X. Zhu, Europhys. Lett. **82**, 17009 (2008).
[6] Z.-A. Ren, W. Lu, J. Yang, W. Yi, X.-L. Shen, Z.-C. Li, G.-C. Che, X.-L. Dong, L.-L. Sun, F. Zhou, and Z.-X. Zhao, Chin. Phys. Lett. **25**, 2215 (2008).
[7] S. Matsuishi, Y. Inoue, T. Nomura, M. Hirano, and H. Hosono, J. Phys. Soc. Jpn. **77**, 113709 (2008).
[8] T. Terashima, M. Kimata, H. Satsukawa, A. Harada, K. Hazama, S. Uji, H. S. Suzuki, T. Matsumoto, and K. Murata, J. Phys. Soc. Jpn. **78**, 083701 (2009).
[9] Z. Ren, Q. Tao, S. Jiang, C. Feng, C. Wang, J. Dai, G. Cao, and X. P. Zhu'an, Phys. Rev. Lett. **102**, 137002 (2009).
[10] C. de la Cruz, Q. Huang, J. W. Lynn, J. Li, W. Ratcliff II, J. L. Zarestky, H. A. Mook, G. F. Chen, J. L. Luo, N. L. Wang, and P. C. Dai, Nature (London) **453**, 899 (2008).
[11] Q. Huang, Y. Qiu, W. Bao, M. A. Green, J. W. Lynn, Y. C. Gasparovic, T. Wu, G. Wu, and X. H. Chen, Phys. Rev. Lett. **101**, 257003 (2008).
[12] Y. Su, P. Link, A. Schneidewind, Th. Wolf, P. Adelmann, Y. Xiao, M. Meven, R. Mittal, M. Rotter, D. Johrendt, Th. Brueckel, and M. Loewenhaupt, Phys. Rev. B **79**, 064504 (2009).
[13] A. I. Goldman, D. N. Argyriou, B. Ouladdiaf, T. Chatterji, A. Kreyssig, S. Nandi, N. Ni, S. L. Bud'ko, P. C. Canfield, and R. J. McQueeney, Phys. Rev. B **78**, 100506(R) (2008).
[14] J. Zhao, Q. Huang, C. de la Cruz, S. Li, J. W. Lynn, Y. Chen, M. A. Green, G. F. Chen, G. Li, Z. Li, J. L. Luo, N. L. Wang, and P. Dai, Nature Mater. **7**, 953 (2008).
[15] J. G. Bednorz and K. A. Mueller, Z. Phys. B **64**, 189 (1986).
[16] R. Marchand and W. Jeitschko, J. Solid State Chem. **24**, 351 (1978).
[17] Z. Ren, Z. Zhu, S. Jiang, X. Xu, Q. Tao, C. Wang, C. Feng, G. Cao, and X. Zhu'an, Phys. Rev. B **78**, 052501 (2008).
[18] H. Raffius, M. Moersen, B. D. Mosel, W. Mueller-Warmuth, W. Jeitschko, L. Terbuechte, and T. Vomhof, J. Phys. Chem. Solids **54**, 135 (1993).
[19] H. S. Jeevan, Z. Hossain, Deepa Kasinathan, Helge Rosner, C. Geibel, and P. Gegenwart, Phys. Rev. B **78**, 092406 (2008).
[20] M. Meven, V. Hutanu, and G. Heger, Neutron News **18**, 19

(2007).
[21] P. Coppens, L. Leiserowitz, and D. Rabinovich, Acta Crystallogr. **18**, 1035 (1965).
[22] J. Rodríguez-Carvajal, Physica B **192**, 55 (1993).
[23] G. J. McIntyre, A. Renault, and G. Collin, Phys. Rev. B **37**, 5148 (1988).
[24] M. A. Tanatar, A. Kreyssig, S. Nandi, N. Ni, S. L. Bud'ko, P. C. Canfield, A. I. Goldman, and R. Prozorov, Phys. Rev. B **79**, 180508(R) (2009).
[25] M. Tegel, M. Rotter, V. Weiss, F. M. Schappacher, R. Poettgen, and D. Johrendt, J. Phys.: Condens. Matter **20**, 452201 (2008).
[26] J. Herrero-Martin, V. Scagnoli, C. Mazzoli, Y. Su, R. Mittal, Y. Xiao, T. Brueckel, N. Kumar, S. K. Dhar, A. Thamizhavel, and L. Paolasini, Phys. Rev. B **80**, 134411 (2009).
[27] T. Yildirim, Phys. Rev. Lett. **101**, 057010 (2008).
[28] M. Reehuis, W. Jeitschko, M. H. Möller, and P. J. Brown, J. Phys. Chem. Solids **53**, 687 (1992).
[29] S. Nandi, A. Kreyssig, Y. Lee, Yogesh Singh, J. W. Kim, D. C. Johnston, B. N. Harmon, and A. I. Goldman, Phys. Rev. B **79**, 100407(R) (2009).
[30] G. Michels, M. Roepke, T. Niemöller, M. Chefki, M. M. Abd-Elmeguid, H. Micklitz, E. Holland-Moritz, W. Schlabitz, C. Huhnt, B. Büchner, A. Wurth, A. Mewis, and V. Kataev, J. Phys.: Condens. Matter **8**, 4055 (1996).
[31] Y. Singh, Y. Lee, B. N. Harmon, and D. C. Johnston, Phys. Rev. B **79**, 220401(R) (2009).
[32] Z. Ren, X. Lin, Q. Tao, S. Jiang, Z. Zhu, C. Wang, G. Cao, and Z. Xu, Phys. Rev. B **79**, 094426 (2009).
[33] E. Dengler, J. Deisenhofer, H.-A. Krug von Nidda, Seunghyun Khim, J. S. Kim, Kee Hoon Kim, F. Casper, C. Felser, and A. Loidl, arXiv:0909.2054 (unpublished).
[34] H. S. Jeevan, Z. Hossain, Deepa Kasinathan, H. Rosner, C. Geibel, and P. Gegenwart, Phys. Rev. B **78**, 052502 (2008).